Scientia Iranica C (2014) 21(6), 2116–2125

Sharif University of Technology
Scientia Iranica
Transactions C: Chemistry and Chemical Engineering
www.scientiairanica.com

Research Note

Lattice Boltzmann relative permeability for CO_2-brine system in a 2D porous medium

S. Mahmoudi[a], **A. Hashemi**[a,*] and **Sh. Kord**[b]

a. *Ahwaz Faculty of Petroleum, Petroleum University of Technology, Ahwaz, Iran.*
b. *Department of Reservoir Engineering, National Iranian South Oil Company, Ahwaz, Iran.*

Received 8 July 2013; received in revised form 21 December 2013; accepted 15 April 2014

KEYWORDS
Relative permeability;
Lattice Boltzmann;
Shan-Chen;
Guo scheme;
CO_2-brine system;
Pore structure;
Capillary number.

Abstract. CO_2 sequestration is a pretty new field with little relevant published data considering the relative permeability of CO_2-brine systems at in-situ conditions. Precise determinations of relative permeability data in gas injection experiments are difficult and expensive; also, several factors affect the accuracy. In this paper, to predict CO_2-brine relative permeability curves, a Shan-Chen type multi-component multiphase lattice Boltzmann model for two-phase flow for a 2D porous medium was developed. Fully periodic and "full-way" bounce back boundary conditions were applied to the model to get infinite domain of fluid with non-slip solid nodes. Incorporation of an external body force was performed by the Guo scheme. The influences of pore structure and capillary number on relative permeability curves were studied in order to establish realistic conditions for investigation of CO_2-brine relative permeabilities. The corrected relative permeability curves for pore structure and capillary number were tangibly in agreement with experimental data.

1. Introduction

In immiscible flow through porous media, a modification of Darcy's law to account the momentum transfer across the interfaces leads to defining an apparent relative permeability, $k_{r,i}$, which is a function of wetting phase saturation, S_w, capillary number, Ca, and viscosity ratio, M [1], and is defined as: "effective permeability divided by permeability to non-wetting phase at minimum wetting phase saturation" [2], given by:

$$u_i = -\frac{k k_{r,i,\mathrm{app}}(S_w, \mathrm{Ca}, M, \nabla P_j)}{\mu_i} \nabla P_i. \qquad (1)$$

The characteristic role of the relative permeability in the estimation of the reservoir performance and ground water transport and remediation in any simulation study and subsequent decision making in reservoir engineering has been a contestable issue. Gas water systems have been studied widely due to their applications in sequestration processes, aquifer pressurizing and WAG injection projects in petroleum and hydrology. CO_2 sequestration is a recently emerging field with little relevant published data regarding the relative permeability of CO_2-brine systems at in-situ conditions [3]. Precise determinations of relative permeability data in gas injection experiments are difficult and expensive; also, several factors affect the accuracy. An alternative approach for this objective is the use of pore-scale modeling like lattice Boltzmann method. The lattice Boltzmann advantage for porous media lies in its ability to incorporate complex boundary conditions relative to continuum modeling approaches and an excellent ability to simulate interfaces between different fluids.

---

*. *Corresponding author. Tel.: +98 21 44222483*
E-mail addresses: mahmoudi.sadegh@gmail.com (S. Mahmoudi); a.hashemi@put.ac.ir (A. Hashemi) and kord1.s@nisoc.ir (Sh. Kord)

Validity verification of relative permeability data, originated from Darcy's law, was one of the subjects of application of multiphase lattice gas and lattice Boltzmann modeling for multi-component oil/water like systems [4]. Some recent efforts to study the gas liquid systems include the works by Yiotis et al. [1] who studied the viscous coupling effects in immiscible two-phase flow in porous media based on the single-component multiphase model of He et al. [5] assuming that the pressure of non-ideal fluids is described by the Carnahan-Starling EOS, the work of Huang et al. [6], and Huang and Lu [7] who studied the relative permeability and coupling effects in steady-state gas-liquid flow in porous media. They used the single component multiphase model of Shan and Chen [8] (like water and its vapor) along with the R-K equation of state to model gas-liquid systems with a high density ratio. They have used the original Shan-Chen scheme for the incorporation of body forces. One recent try to use the LB method for CO_2-brine systems is the work by Suekane et al. [9] who were studying the Behavior of supercritical CO_2 injected into porous media containing water. They implemented the Free Energy model of swift et al. [10] to simulate CO_2-rich channels running through water-rich regions.

In the current study, multi-component multiphase Shan-and-Chen-type lattice Boltzmann model was used in order to study apparent relative permeabilities of gas-liquid systems. This type of modeling is suitable for flow simulation of different fluid pairs such as CO_2 and brine with essentially different kinematic viscosity values.

An outline of the paper goes as follows. After a brief review of the theory of the LB method, the validity verifications of the model for fluid flow in a few simple pore geometries are reviewed. The influence of pore structure and capillary number on relative permeability curves is also studied in order to establish realistic stable conditions. The CO_2-brine relative permeability curves are then calculated as a function of wetting fluid saturation, viscosity ratio and for a specific capillary number and compared with some experimental results. The concluding remarks are presented afterward.

2. Theory, background and model setup

In LB method and 2D models, the domain is divided into regular lattices with the same spacing in both x and y directions and at each lattice site, a distribution function $f_m^\sigma(x,y,t)$ is defined that denotes the number of particles of fluid σ at site (x,y) in the direction of m with velocity e_m. During each time step, streaming and collisions of these particles are performed through the Boltzmann equation. The discretized form of Boltzmann equation with the assumption of BGK (Bhatnagar-Gross-Krook) reads:

$$\frac{\partial f_i}{\partial t} + e_i \frac{\partial f_i}{\partial x} = \frac{f_i - f_i^{\mathrm{eq}}}{\tau}. \tag{2}$$

By the Euler's expansion of the derivatives in Eq. (2), one can obtain the forms:

$$f_\alpha(x + e_\alpha \Delta t, t + \Delta t) = f_\alpha(x,t) - \frac{f_\alpha(x,t) - f_\alpha^{\mathrm{eq}}(x,t)}{\tau} + \Delta t.F, \tag{3}$$

$$f_\alpha^{\mathrm{eq}}(x) = w_\alpha \rho(x) \left[1 + \frac{e_\alpha . u^{\mathrm{eq}}}{c_s^2} + \frac{u^{\mathrm{eq}} u^{\mathrm{eq}} : \left(e_\alpha e_\alpha - c_s^2 I \right)}{c_s^4} \right], \tag{4}$$

$$u^{\mathrm{eq}} = u + \Delta u = u + \frac{\tau F}{\rho}, \tag{5}$$

$$w_1 = \frac{4}{9}, \qquad w_{2345} = \frac{1}{9}, \qquad w_{6789} = \frac{1}{36}.$$

The macroscopic fluid density is the sum of the discrete values of the distribution function:

$$\rho = \sum_{\alpha=1}^{9} f_\alpha. \tag{6}$$

The macroscopic velocity u is an average of the microscopic velocities e_m weighted by the discrete values of the distribution function f_m as:

$$u = \frac{1}{\rho} \sum_{\alpha=1}^{9} f_\alpha e_\alpha. \tag{7}$$

The fluid kinematic viscosity is defined as:

$$\nu = \frac{1}{6}(2\tau - 1), \qquad \tau > 0.5. \tag{8}$$

In order to simulate multiphase systems, forces between two different phases including fluid-fluid and fluid-solid forces should be incorporated in the model. By introducing the second species in the model in the form of a multi-component multiphase model, previous equations should be slightly modified. In such a case, equilibrium velocity for fluid phase σ is defined as:

$$u_\sigma^{\mathrm{eq}} = u' + \frac{\tau_\sigma F}{\rho_\sigma}, \tag{9}$$

$$F = F_{\mathrm{cohesion}} + F_{\mathrm{adsorption}} + F_{\mathrm{external}},$$

$$u' = \left(\sum\nolimits_\sigma \sum\nolimits_{\alpha=1}^{9} f_\alpha^\sigma e_\alpha / \tau_\sigma \right) / \left(\sum\nolimits_\sigma \rho_\sigma / \tau_\sigma \right). \tag{10}$$

The composite velocity u' is a measure of the whole fluid velocity (or total composite velocity) and is defined as [11]:

$$u = u' + F/(2\rho), \quad \text{with} \quad \rho = \sum_{\sigma} \rho_\sigma. \tag{11}$$

Also, the whole fluid kinematic viscosity can be computed as:

$$\nu = \left(\sum_{\sigma} x_\sigma \tau_\sigma - 0.5 \right) /6, \quad \text{with} \quad x_\sigma = \rho_\sigma/\rho, \tag{12}$$

while the cohesion and adsorption forces are given by:

$$F_c(x,t) = -G_c \psi_\sigma(x,t) \sum_{\alpha=1}^{9} w_\alpha \psi_{\overline{\sigma}}(x + e_\alpha \Delta t, t) e_\alpha, \tag{13}$$

$$F_{\text{ads}}(x,t) = -G_{\text{ads}} \psi(x,t) \sum_{\alpha=1}^{9} w_\alpha S(x + e_\alpha \Delta t) e_\alpha, \tag{14}$$

with σ and $\overline{\sigma}$ denoting two different fluids, and G_c and G_{ads} used to control the IFT and the surface wettability. In the above equations ψ and S are the potential function and an indicator of solid sites (1) or pore sites (0), respectively [12].

Owing to the nature of the interaction between two fluids, smaller values of G_s lead to diffused interfaces, whereas larger values lead to sharp interfaces and purer components. However, in the later case, the simulation will suffer from numerical instability after some critical values. The sign of these parameters indicate the repulsion or attraction nature of the forces and their absolute value can be adjusted to model the desired IFT and contact angles.

For the EOS proposed by Shan and Chen, the effective (number) density ψ is:

$$\psi(\rho) = \rho_0 \left[1 - \exp\left(-\frac{\rho}{\rho_0} \right) \right], \tag{15}$$

where ρ_0 is an arbitrary constant (initial density), here taken as 1.2 mu/lu^2.

External body force was incorporated through the Guo scheme, since Guo et al. [13] have already demonstrated the best procedure to accommodate the LBM with continuity and momentum equations on the macroscopic scale (i.e., Navier-Stokes equation). In Guo's scheme we have:

$$F_i = \left(1 - \frac{1}{2\tau} \right) w_i \left[\frac{(e_i - u)}{c_s^2} + \frac{e_i(e_i.u)}{c_s^4} \right] .F. \tag{16}$$

This term needs to be added into the collision operator and also the velocity needs to be shifted as:

$$u^{\text{eq}} = \frac{1}{\rho} \sum_{i=1}^{9} f_i e_i + F\Delta t/(2\rho). \tag{17}$$

'Full way' bounce back scheme and fully periodic boundaries have been applied at the solid and non-solid boundaries of the domain, respectively, to simulate an infinite domain of fluid. The "bounce-back" method is applied to simulate the non-slip boundaries at the solid nodes (the usual practice in classic fluid dynamics) and in periodic boundary condition, nodes on the opposite boundary are simply considered as the neighboring points of the boundary nodes.

3. Results and discussion

3.1. Model verification

The conventional procedure for verifying LB models is the primary bubble and contact angle tests proceeded by the channel flow simulation for investigation of Poiseuille flow pattern [1,4]. For simulation of relative permeability curves, we do need to simulate single phase flow too. A simple verification of single phase models is the model ability to predict the absolute permeability of a simple porous media like ideal sphere packs.

3.1.1. Sphere pack porous media

A simple and primary benchmark to the model is the ability to predict the Darcy's permeability of a simple pore structure like sphere pack model. For this purpose, a sand pack was considered as the sphere pack to be applied to the model through Kozeny-Carman correlation [14]:

$$k = \frac{\phi^3 d^2}{36kc(1-\phi)^2}. \tag{18}$$

Here, kc is the Kozeny-Carman constant, being an empirically measured factor which represents both the shape factor and the deviation of flow direction from that in a duct. For beds packed with spherical particles $kc = 5$. The sand pack was prepared at the reservoir rocks laboratory of Petroleum University in Iran with 1 m length and 5 cm diameter. The measured porosity and water permeability were 26% and 1.44 D, respectively. These properties along with the Kozeny correlation produced a grain size of 0.09 mm which was taken as the characteristic length to be applied in the model. 26% porosity implies that rhombohedral-pack spheres model should be implemented.

For Darcy flow, one has:

$$k = -\frac{U\mu}{dp/dx}. \tag{19}$$

To relate the permeability to units measured in the LB simulation, we apply the force balance condition:

$$x\text{Body}.x^3 = (P_{\text{in}}. - P_{\text{out}}).x^2 = -(dP/dx)x^3. \tag{20}$$

From Eq. (20), and by applying $dp/dx = -x$ Body we obtain:

$$k = \frac{U\nu\rho}{x\text{Body}}. \tag{21}$$

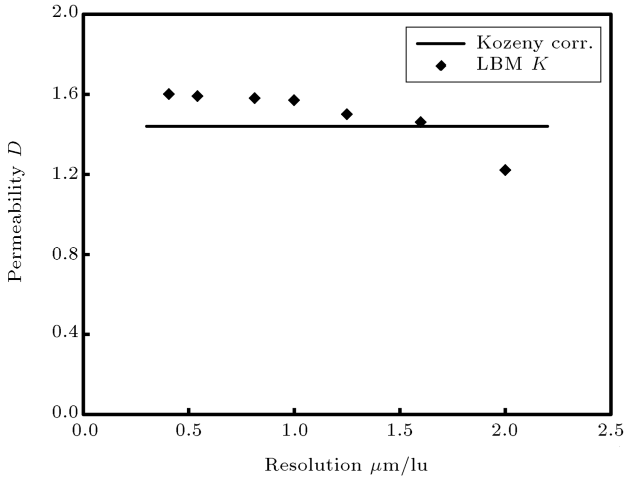

Figure 1. Kozeny-Carman and LBM permeability.

For the characteristic length considered here, every 615 lattice units (lu) represent 1 mm in physical domain, so for the porous medium with sphere diameter of 55 lu we have 55/615 = 0.09. To convert the LB permeability to physical permeability, we took (0.001 m/615 lu)^2.k_{LB}.

As mentioned in Huang et al. [15], for single phase flow, the permeability of the porous medium is slightly dependent on τ when the BGK model is used for the collision term; so the fluid fluxes can be calculated for the specified G_c and τ. Simulation results (for $\tau = 1$ and $\rho = 1$ mu/lu^2) show good agreement with Kozeny correlation with less than 10% error, as the resolution increases. However, the obtained precision is acceptable relative to the difference exists between various correlations. The estimated lower LBM permeability at lower resolution is rooted in the roughness effect of digital images in representation of the sphere surface with a finite number of solid sites that cause the spheres appear somewhat jagged which results in a kind of barrier to flow (Figure 1).

3.1.2. IFT and contact angle

Whenever the Shan and Chen type lattice Boltzmann model is applied a necessary part of analyses is the bubble test. The reason is that in the SC model, the interfacial tension is not a direct input and the strength of surface tension is controlled by the parameter G_c. The same reason stands for wetting characteristic of solids that is controlled by the parameter G_{ads} through contact angle test.

In multi-component LB models, the bubble tests check the ability of the model in relating the pressure difference, radius of curvature and interfacial tension when a bubble of one fluid is immersed in another fluid as:

$$\Delta p = \frac{\gamma}{R}. \tag{22}$$

The pressure at position x can be determined from the

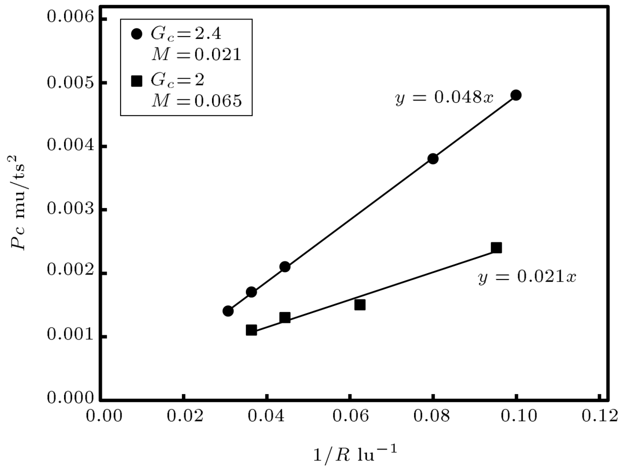

Figure 2. IFT simulation for small fluid densities.

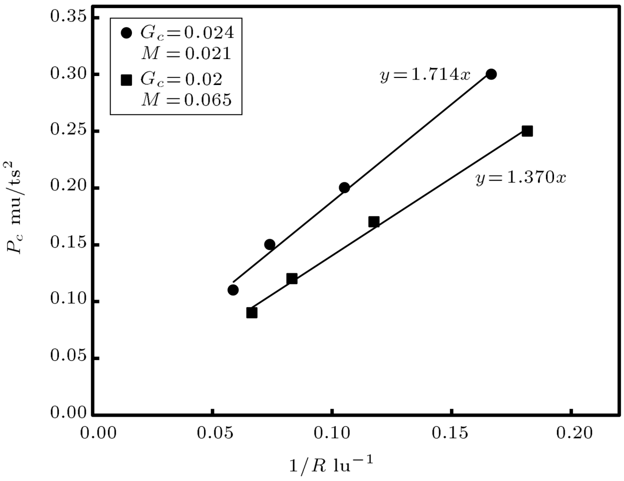

Figure 3. IFT simulation for 40 times larger fluid densities.

densities [16]:

$$P(x) = \frac{1}{3}(\rho_1(x) + \rho_2(x)) + \frac{1}{3}G_c\psi_1(x)\psi_2(x). \tag{23}$$

In this test, various initial radii bubbles of less viscous fluid was placed in a domain of size 150 lu × 150 lu for two sets of density values (one 0.9/1.0 and another 0.9/3.5) and two different viscosity ratios (0.021 and 0.065). The viscosity ratio was computed as $M = \mu_{\text{nw}}/\mu_w = \nu_{\text{nw}}\rho_{\text{nw}}/(\nu_w\rho_w)$ as Figures 2 and 3 also comply.

The contact angle test demonstrates the ability to model different wetting behavior, also verifying the assumption of direct relationship between cohesion and adsorption parameters and the interfacial tension values in Young's equation (Eqs. (24) and (25)) [12]. Eqs. (26) and (27) were applied to compute the contact angle of a drop on a surface with the parameters R, L and H being the drop radius, drop base and drop height, respectively [16], given by:

$$\gamma \cos\theta = (\gamma_{S2} - \gamma_{S1}), \tag{24}$$

$$\cos\theta = \frac{G_{\text{ads2}} - G_{\text{ads1}}}{G_c}, \tag{25}$$

$$R = \frac{4H^2 + L^2}{8H}, \tag{26}$$

$$\tan\theta = \frac{L}{2(R-H)}. \tag{27}$$

In contact angle tests, a drop of 30 lu diameter of wetting fluid was placed in a domain of size 120 lu × 150 lu surrounded by non-wetting fluid. According to Huang et al. [16], when $G_c\rho_i > 2$, the compressibility effect of LBM increases; this causes some deviation from the direct relationship between cohesion and adsorption parameters and the interfacial tension values in Young's equation. Based on our simulations, for a specific density ratio (for example $0.90/1.0 = 40/45$) the choice of the density values itself is a cause of distortion from the linear trend of contact angles versus the drop adsorption $G_{\text{ads1}}(G_c\rho_i < 2)$. This factor constrains the proper possible choices of the cohesion parameter in a way that if larger density values are selected, smaller values of G_c must be assigned, and hence the adhesion parameters will become several times larger than cohesion that subsequently violate the cosine definition in Eq. (25). But, an exciting effect of large density values and low cohesion parameter is that a larger IFT was obtained - which is preferred in flow simulations due to sharp interfaces and purer components - as shown in Figures 2 and 3. For small density values and $G_c\rho_i > 2$, S-shape relationship and for $G_c\rho_i < 2$ a linear relationship between the contact angle and the adhesion parameter were detected, as shown in Figures 4 and 5.

3.1.3. Two-phase flow in a 2D channel

To check the model ability to simulate multiphase flow problems, we investigated the Poiseuille pattern in a 2D channel. Due to periodicity, a 121 lu × 11 lu domain was considered to reduce the computational cost and the rather thick interface (6-8 lu) effect in SC model. By the analytical solution of Poiseuille flow in a channel, the corresponding relative permeability for wetting and non-wetting phases is [1]:

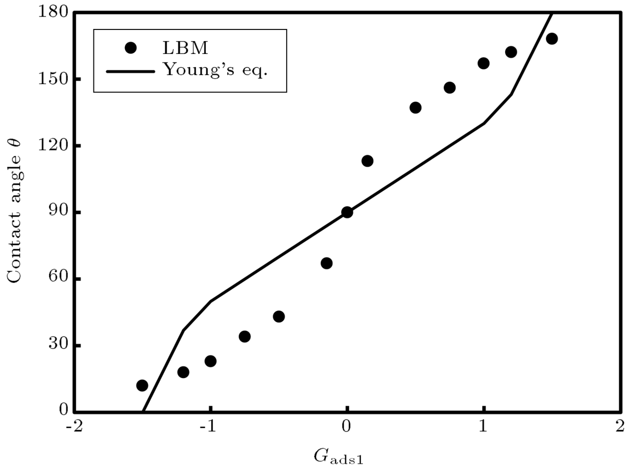

Figure 4. Calculated contact angles as a function of the drop adsorption parameter, G_{ads1}, for $G_c\rho i > 2$.

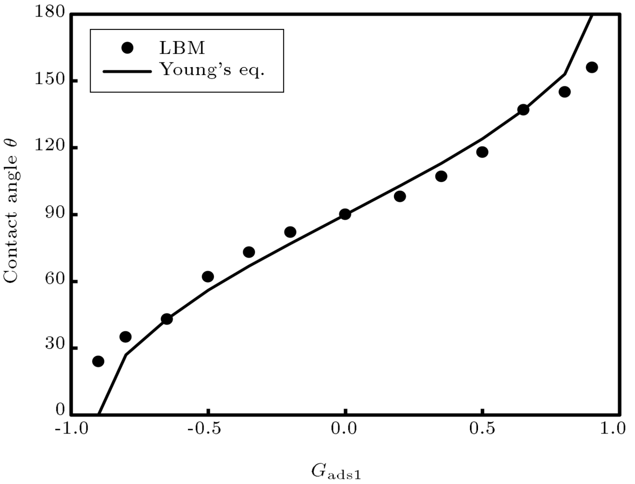

Figure 5. Calculated contact angles as a function of the drop adsorption parameter, G_{ads1} for $G_c\rho i < 2$.

$$k_{r,w} = \frac{1}{2}S_w^2(3 - S_w), \tag{28}$$

$$k_{r,\text{nw}} = S_{\text{nw}}\left[\frac{3}{2}M + S_{\text{nw}}^2\left(1 - \frac{3}{2}M\right)\right], \tag{29}$$

where S_w is defined as $S_w = 1 - a/b$ with $2b$ and a being the channel width and the location of the interface relative to the central line of the channel, respectively. LBM relative permeability was calculated at the outlet face defined as the cumulative flux of one fluid divided by the fluid flux when only that fluid exists in the domain. This method is applicable when Darcy's law conditions are satisfied which implies that low Reynolds number and steady state (constant saturation) conditions are reached.

These simulations were performed with tau values 0.75 and 1.17, $G_c = 3$ and $G_{\text{ads}} = 1.5$. The IFT and contact angle values were calculated as $\sigma = 0.042$ mu.lu/ts^2 and $\theta = 9^\circ$; capillary number, Ca, can be regarded as the ratio of the body forces to the interfacial forces [17]. In this study, F_{ext} was a uniform steady body force, here equal to 1.2×10^{-8} mu/(lu.ts^2) that resulted in $\text{Ca} = 1.2 \times 10^{-8}/0.042 = 2.8 \times 10^{-7}$. The Reynolds number was also maintained low to ensure the applicability of Darcy's law, with the maximum lattice velocity of 0.00014 lu/ts and kinematic viscosity of 0.167 lu^2/ts and 20 lu pore diameter, resulting thus in $\text{Re} = Ud/\nu = 0.017$.

In a situation where the more viscous fluid is the wetting phase, the relative permeability of wetting and

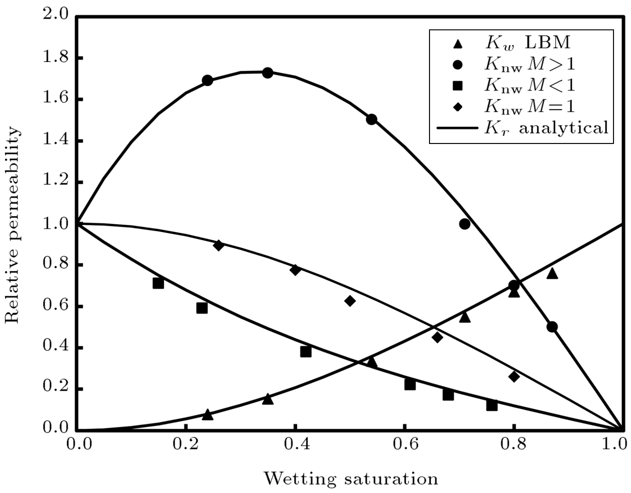

Figure 6. Comparison of LB modelling results and analytical solution for variation of relative permeabilities with respect to saturation ratio in two-phase Poiseuille flow.

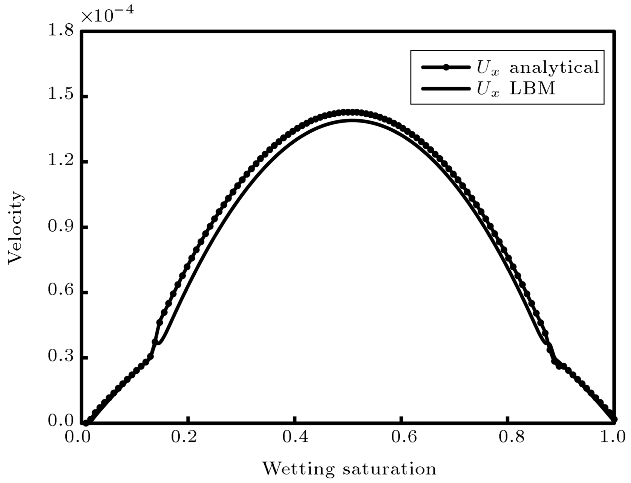

Figure 7. Velocity profile in the channel, comparison of LB modelling results and analytical solution of Poiseuille flow.

non-wetting fluids obey the conventional pattern with the non-wetting relative permeability greater in magnitude. Figure 6 shows the analytical and simulation results. The velocity profile is also shown in Figure 7.

Since the relative permeability of wetting fluid is not a function of the viscosity ratio, when the viscosity of the wetting phase is less than that of non-wetting, no change will be made on its curve, but the non-wetting fluid experiences a lubricating effect during the flow and shows a relative permeability greater than unity. Good agreement between analytical and simulation results were observed.

3.2. Two-phase flow through porous media

In simulation of multiphase systems, the typical porosity is somewhat greater than 50%. The first reason is to get percolating systems in all directions, and secondly, to reduce the effect of the interface's thickness and to reduce the influence of pore structure on the results [1]. Another alternate for these objectives is to increase the resolution of the medium (reducing μm/lu). But increase in computational cost or in other words high performance computing hardware requirement is the drawback. Another limit of low porosity mediums is the threshold capillary number. The lower the porosity, the larger the Ca required, getting a percolating system.

Using a MATLAB code, simulation of a 200×200 lu^2 domain with 47% porosity and for 40000 ts, takes about 1 hour to complete. Our simulations were operated on a computer with a 3 GHz Intel processor and 1 GB RAM.

Considering the number of simulations needed for parameter optimization (G_c and τ) and investigation of relative permeability, to reduce the computational cost and getting a percolating system, we implemented a 150×150 lu^2 domain with about 60% porosity and a capillary number in the range of $10^{-3} - 10^{-4}$. We remember that the simple periodic boundary condition easily compensated the small domain size by repeating the domain at each time step. In the case of other boundaries, using extensively large domains is necessary to get meaningful results.

Two initialization methods for saturation distribution can be considered; a random distribution and an injection like initial saturation. The first case is suitable for a pair fluid with large density difference to gain stability and the second is more realistic in injection processes. Utilizing the mentioned boundary condition and the initial condition of the less viscous fluid being injected into the medium, we have calculated the relative permeabilities at different cross sections to get an average value.

A micro model was implemented to construct the porous medium of our simulations. The micro model has been engineered at Schlumberger Cambridge Research, based on a thin section of a 3D Berea sand stone rock sample (typically with 22% porosity) [18]. However, the micro model shows 33% porosity.

We reproduced a symmetric image relative to $x-y$ axes using a piece of size 569 μm × 891 μm of the micro model and subsequently, a more simplified image was derived from the symmetric image which is compared with the ideal sphere pack model (Figures 8 and 9).

In all simulations, the primary constant saturation throughout the medium was attained after 10000 ts, however, we assumed the steady state condition after 30000 ts.

The applied technique has the advantage to simulate any fluid pair with $M > 0.02$ in any medium including: porous media, capillaries, and surfaces with adsorptive or non-wet characteristic. But all

Table 1. CO_2-brine system properties by Perrin et al. (2008).

Pressure (psia)	Temp. °F	Flow rate cc/min	Viscosity (cp)		Densities (g/cc)		S. St. Core porosity	Capillary number
			Brine	CO_2	Brine	CO_2		
1800	120	1.2	0.558	0.046	0.99	0.56	0.22	5×10^{-6}

Table 2. CO_2-brine system properties in LBM.

Cohesion G_c	Adsorption G_{ads}	Time steps	Tau values (τ)		Densities mu/lu^2		Model porosity	Capillary number
			Brine	CO_2	Brine	CO_2		
3	1.5	30000	1.2	0.6	1.76	1	0.66	1.2×10^{-3}

Table 3. LBM properties in investigation of the influence of pore structure on the relative permeability.

	Cohesion G_c	Adsorption G_{ads}	Time steps	Tau values (τ)		Densities mu/lu^2		Model porosity	Capillary number
				Liquid	Gas	Liquid	Gas		
1	3	1.5	30000	1.17	0.55	1.15	1	0.38	4.7×10^{-3}
2	3	1.5	30000	1.8	0.55	1.7	1	0.38	4.7×10^{-3}

Figure 8. Simplified pore structure, 264 lu × 502 lu, 38% porosity.

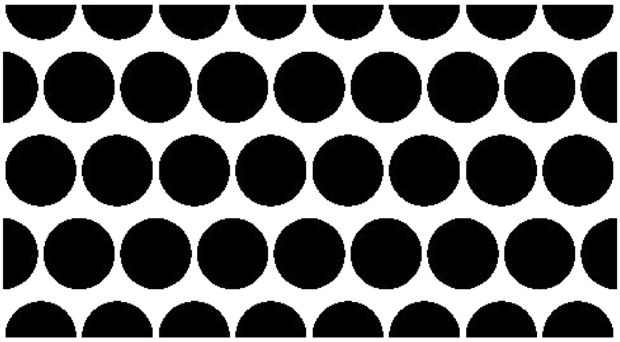

Figure 9. Ideal sphere pack model, 262 lu × 484 lu, 38% porosity.

applications of the LBM will remain at the core scale not reservoir scale.

3.2.1. CO_2-brine system

To simulate CO_2-brine systems, we implemented low viscosity ratio pair fluids with the desired Ca and density ratio such that the simulated in-situ conditions match the experimental conditions. Since in the laboratory tests and for strongly water wet system when viscous forces dominated, it is reasonable to ignore capillary pressure except to set an initial saturation condition and also gravitational effects are negligible [2] we can expect the results to be independent to bond number and dependent only to the pore structure and capillary number. The results then should be corrected for pore structure and capillary number. The CO_2-brine data used here were selected from Perrin et al. [19] as reported by Table 1. The LB model properties for this system are presented by Table 2.

3.2.2. Pore structure

To investigate the influence of pore structure and Ca on the relative permeability curves, the response of the micro model porous media was compared with corresponding porosity and permeability, ideal sphere pack structure and for three values of Ca, respectively.

In exploring the influence of pore structure, the two sets of parameters reported in Table 3 were used to show the model ability to simulate low viscosity ratio gas liquid systems, and also to investigate any dependency of the results on the viscosity sets. Figures 10 and 11 illustrate the influence of pore structure. The labels 1 and 2 in these figures identify the micro model and the ideal sphere pack model responses, respectively. As it has been illustrated therein, an increase in surface area increased the non-wetting phase relative permeability, but almost did not alter the wetting phase relative permeability. For wetting phase saturations below 40% and by 50% increase in surface area, both of these simulations have shown an average deviation of 55% for non-wetting phase relative permeability.

3.2.3. Capillary number

The capillary number, Ca, has been set to the three values 2.1×10^{-3}, 1.2×10^{-3} and 6×10^{-4}, to investigate its influence on the relative permeability curves (using the

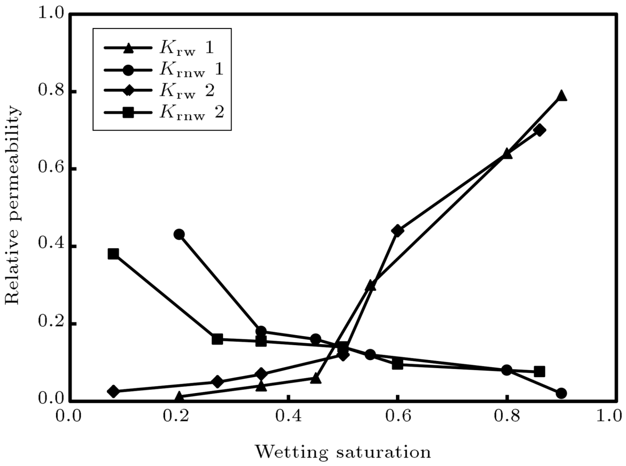

Figure 10. LB relative permeability for $M = 0.065$, $\sigma = 0.021$ and $\mathrm{Ca} = 4.7 \times 10^{-3}$; 1 indicates the micro model and 2 the sphere pack.

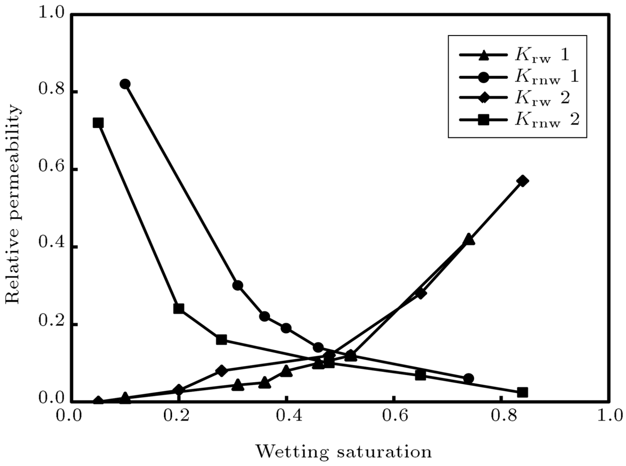

Figure 11. LB relative permeability for $M = 0.021$, $\sigma = 0.048$ and $\mathrm{Ca} = 4.7 \times 10^{-3}$; 1 indicates the micro model and 2 the sphere pack.

properties in Table 2) for CO_2-brine system. Moreover, porosity is chosen as 66% to obtain higher precision and less dependency to the pore structure in an ideal sphere pack medium. Figure 12 demonstrates this issue. As an average, for a reduction of 45% in capillary number, the wetting phase relative permeability has been reduced by 30% and a reduction of 72% in Ca lower the non-wetting fluid relative permeability by 30%.

3.2.4. *Comparative study*

The pore structure and capillary number can now be corrected to properly simulate the laboratory condition and compare the results. 66% porosity medium needs 40% increase in surface area to be a 33% porosity one (corresponding to 22% porosity sand stone with 33% porosity micro model). The capillary number should be lowered by 99.6% to get 5×10^{-6}. After reducing the wetting and non-wetting phase's relative permeability by 66% and 85%, respectively, the resulted curves are as shown in Figure 13.

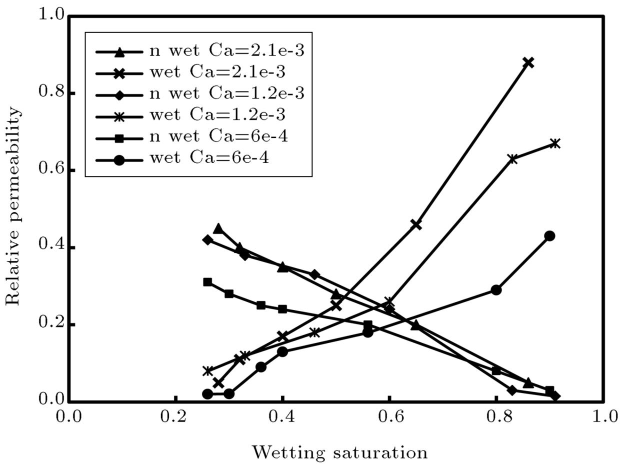

Figure 12. Investigation of capillary number influence on relative permeability.

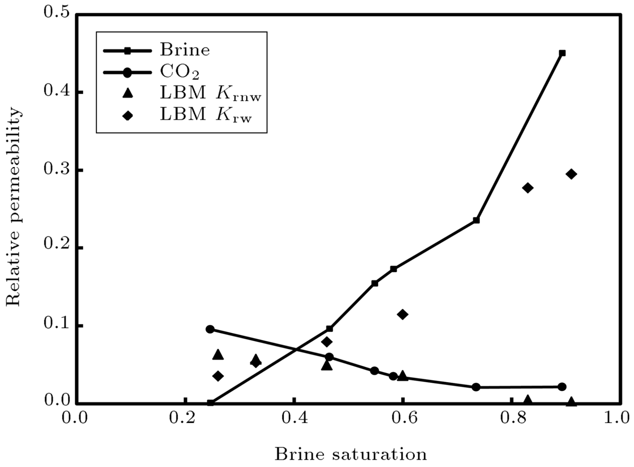

Figure 13. CO_2-brine relative permeability by Perrin et al. (2008) and LBM simulation.

4. Concluding remarks

In this paper, a multi-component multiphase Shan-Chen type LB model was used to study the two-phase flow in porous media and to simulate CO_2-brine relative permeability curves in a realistic pore structure. For small density values, when $G_c\rho_i > 2$, S-shape relationship, and for $G_c\rho_i < 2$, a linear relationship between the contact angle and the adhesion parameter was detected. The predicted relative permeability curves were tangibly in agreement with experimental data by involving the pore structure and capillary number effects. The applied technique has the advantage to simulate any fluid pair with $M > 0.02$ in any medium including: porous media, capillaries, and surfaces with adsorptive or non-wet characteristic.

Acknowledgement

We gratefully acknowledge the financial support for this research by the National Iranian South Oil Company (NISOC).

Nomenclature

BGK	Bhatnagar-Gross-Krook single relaxation time collision operator
Ca	Capillary number
IFT	Interfacial tension
LB	Lattice Boltzmann
LBM	Lattice Boltzmann Modeling
SC	Shan and Chen
WAG	Water Alternate Gas injection
xBody	Body force in x direction

Scripts

ads	Adsorption
app	Apparent
c	Cohesion
cw	Connate water
d	Drop
e	Effective
eq	Equilibrium
ext	External
int	Inter particle
nw	Non-wet
r	Relative
w	Wet
α	Direction indicator
σ	Phase indicator

Latin symbols

c	Basic lattice speed of particles equal to 1 (lu/ts)
c_s	The sound speed of the model equals to $c/\sqrt{3}$
d	Pore diameter (lu)
F	Body force (mu/(lu.ts^2))
F_{ext}	External body force (mu/(lu.ts^2))
F_{int}	Inter particle force (mu/(lu.ts^2))
F_{ads}	Adsorption force (mu/(lu.ts^2))
f_α	Directional density (local distribution function)
f_α^{eq}	Local equilibrium distribution function
G	Strength of interaction forces (1/ts)
G_{ads}	Strength of adsorption forces to control surface wettability (1/ts)
G_c	Strength of cohesion forces to control interfacial tension (1/ts)
g	Gravitational force (lu/ts^2)
H_d	Drop's height on a surface (lu)
k	Permeability (D)
k_r	Relative permeability-dimensionless
k_e	Effective permeability (D)
$k_{r(\text{app})}$	Apparent relative permeability-dimensionless
L	Length (lu)
L_d	Drop base (lu)
lu	Lattice unit
M	Viscosity ratio-dimensionless
mu	Mass unit
P	Pressure (mu/ts^2)
Pc	Capillary pressure (mu/ts^2)
R_d	Drop radius (lu)
S	Saturation- fraction
t	Time (ts)
ts	Time step
U	Darcy velocity (m/s)
u	Macroscopic velocity (lu/ts)
u'	Composite (hole fluid) velocity (lu/ts)
w_α	Directional weighting multiplier
x	x coordinate

Greek symbols

Δ	Delta operator
ϕ	Porosity
γ	Young-Laplace interfacial tension (dyne/cm)
μ	Dynamic viscosity (cp)
ν	Kinematic viscosity (lu^2/ts)
θ	Contact angle (degree)
ρ	Average density (mu/lu^2)
σ	Interfacial tension (mu.lu/ts^2)
τ	Relaxation time (ts)
Ω	Collision operator
ψ	Potential function (mu/lu^2)

References

1. Yiotis, A.G., Psihogios, J. and Kainourgiakis, M.E. "A lattice Boltzmann study of viscous coupling effects in immiscible two-phase flow in porous media", *Colloids and Surfaces A: Physicochem. Eng. Aspects*, **300**, pp. 35-49 (2007).

2. Archer, J.S. and Wall, C.G. “Relative permeability and multiphase flow in porous media”, In *Petroleum Engineering, Principles and Practice*, pp. 102-121, Graham and Trotman Ltd, London (1986).
3. Bennion, D.B. and Bachu, S. “Dependence on temperature, pressure, and salinity of the IFT and relative permeability displacement characteristics of CO_2 injected in deep saline aquifers”, SPE 102118 (2006).
4. Sukop, M.C. and Or, D. “Lattice Boltzmann method for modeling liquid-vapor interface configurations in porous media”, *Water Resources Research*, **40**, pp. 1509-1514 (2004).
5. He, X., Chen, S. and Zhang, R. “A lattice Boltzmann scheme for incompressible multiphase flow and its application in simulation”, *Journal of Computers and Physics*, **152**(2), pp. 642-663 (1999).
6. Huang, H., Li, Z., Liu, S. and Lu, X. “Shan-and-Chen-type multiphase lattice Boltzmann study of viscous coupling effects for two-phase flow in porous media”, *Int. J. Numer. Meth. Fluids*, **61**(3), pp. 341-354 (2008).
7. Huang, H. and Lu, X. “Relative permeabilities and coupling effects in steady-state gas-liquid flow in porous media: A lattice Boltzmann study, physics of fluids”, **21**, pp. 92104-92112 (2009).
8. Shan, X. and Chen, H. “Lattice Boltzmann model for simulating flows with multiple phases and components”, *Physical Review E*, **47**(3), pp. 1815-1819 (1993).
9. Suekane, T., Soukawa, S., Iwatani, S., Tsushima, S. and Hirai, S. “Behavior of supercritical CO_2 injected into porous media containing water”, *Energy*, **30**, pp. 2370-2382 (2005).
10. Swift, M.R., Osborn, W.R. and Yeomans, J.M. “Lattice Boltzmann simulation of non-ideal fluids”, *Physical Review Letters*, **75**, pp. 830-833 (1995).
11. Shan, X. and Doolen, G. “Diffusion in a multi component lattice Boltzmann equation mode”, *Physical Review E*, **54**, pp. 3616-3620 (1996).
12. Sukop, M.C. and Thorne, D., *Lattice Boltzmann Modeling: An Introduction for Geoscientists and Engineers*, Springer, New York (2007).
13. Guo, Z., Zheng, C. and Shi, B. “Discrete lattice effects on the forcing term in the lattice Boltzmann method”, *Physical Review E*, **65**, pp. 463081-463086 (2002).
14. Kaviany, M., *Principles of Heat Transfer in Porous Media*, Springer, New York (1995).
15. Huang, H., Wang, L. and Lu, X. “Evaluation of three lattice Boltzmann models for multiphase flows in porous media”, *Computers and Mathematics with Applications*, **61**, pp. 3606-3617 (2011).
16. Huang, H., Thorne, D.T., Jr. Schaap, M.G. and Sukop M.C. “Proposed approximation for contact angles in Shan-and-Chen-type multi component multiphase lattice Boltzmann models”, *Physical Review E*, **76**, pp. 66701-66706 (2007).
17. Rothman, D.H. and Keller, J.M. “Immiscible cellular-automaton fluids”, *Journal of Statistical Physics*, **52**, pp. 1119-1127 (1988).
18. Boek, E.S. and Venturoli, M. “Lattice-Boltzmann studies of fluid flow in porous media with realistic rock geometries”, *Computers and Mathematics with Applications*, **59**, pp. 2305-2314 (2010).
19. Perrin, J.C., Krause, M. and Benson, S.M. “Relative permeability properties of the CO_2/brine system in saline aquifers: An experimental study”, *Seventh Annual Conference on Carbon Capture & Sequestration*, Pittsburgh, Pennsylvania (2008).

Biographies

Sadegh Mahmoudi is a Master of Science student at PUT, ranking the first among the reservoir engineering students. He received a BSc in Petroleum Engineering from PUT in 2011, while ranking second among the production engineering students. He has been a student member of EAGE (European Association of Geoscientist & Engineers) from 2010 to 2011. Job trainings at the Iranian Offshore Oil Company (I.O.O.C), and Petroleum Engineering Department of NISOC were some of his educational experiences.

Abdolnabi Hashemi is an Assistant Professor of Petroleum Engineering and Dean of Tehran Faculty of Petroleum at Petroleum University of Technology, (PUT). He holds a PhD in Petroleum Engineering form Imperial College London in 2005. Before joining PUT in 2006, he held a variety of senior technical and management positions with the National Iranian South Oil Company (NISOC).

Shahin Kord is a senior reservoir engineer with the National Iranian South Oil Company (NISOC). He currently acts as the technical head of the EOR division at reservoir engineering department of NISOC. He holds a BSc degree in Petroleum Reservoir Engineering from Petroleum University of Technology (PUT) working on using polymers as EOR agent, Iran, 1998. He also received MSc and PhD degree in Chemical and Petroleum Engineering from Shiraz University focusing on water/gas coning and Asphaltene Precipitation and deposition, Iran, 2000 and 2012. He has in-depth experience in different aspects of Petroleum Reservoir Engineering such as rock type analysis, PVT, reservoir fluid characterization, full-field reservoir simulation, and MDP as well as programming and application of Reservoir Engineering softwares.